The role of microplastics in microalgae cells aggregation: a study at the molecular scale using atomic force microscopy

Irem Demir-Yilmaz, Nadiia Yakovenko, Clément Roux, Pascal Guiraud, Fabrice Collin, Christophe Coudret, Alexandra ter Halle, Cécile Formosa-Dague

The role of microplastics in microalgae cells aggregation: a study at the molecular scale using atomic force microscopy

Irem Demir-Yilmaz,[a,b] Nadiia Yakovenko,[c] Clément Roux,[c] Pascal Guiraud,[a,d] Fabrice Collin,[c] Christophe Coudret,[c,d] Alexandra ter Halle,[c] and Cécile Formosa-Dague,[a,d*]

[a] TBI, Université de Toulouse, INSA, INRAE, CNRS, Toulouse, France.

[b] LAAS, Université de Toulouse, CNRS, Toulouse, France.

[c] UMR 5623 IMRCP, CNRS, Toulouse, France.

[d] Fédération de Recherche Fermat, CNRS, Toulouse, France.

*corresponding author: Cécile Formosa-Dague, formosa@insa-toulouse.fr
INSA de Toulouse, Toulouse Biotechnology Institute
135 avenue de Rangueil,
31400 Toulouse, France

Abstract

Plastic pollution has become a significant concern in aquatic ecosystems, where photosynthetic microorganisms such as microalgae represent a major point of entry in the food chain. For this reason an important challenge is to better understand the consequences of plastic pollution on microalgae and the mechanisms underlying the interaction between plastic particles and cell's interfaces. In this study, to answer such questions, we developed an interdisciplinary approach to investigate the role of plastic microparticles in the aggregation of a freshwater microalgae species, *Chlorella vulgaris.* First, the biophysical characterization, using atomic force microscopy, of the synthetic plastic microparticles used showed that they have in fact similar properties than the ones found in the environment, with a rough, irregular and hydrophobic surface, thereby making them a relevant model. Then a combination of optical imaging and separation experiments showed that the presence of plastic particles in microalgae cultures induced the production of exopolysaccharides (EPS) by the cells, responsible for their aggregation. However, cells that were not cultured with plastic particles could also form aggregates when exposed to the particles after culture. To understand this, advanced single-cell force spectroscopy experiments were performed to probe the interactions between cells and plastic microparticles; the results showed that cells could directly interact with plastic particles through hydrophobic interactions. In conclusion, our experimental approach allowed highlighting the two mechanisms by which plastic microparticles trigger cell aggregation; by direct contact or by inducing the production of EPS by the cells. Because these microalgae aggregates containing plastic are then consumed by bigger animals, these results are important to understand the consequences of plastic pollution on a large scale.

Keywords: microplastic, microalgae, aggregation, interaction, atomic force microscopy

1. Introduction

Plastic is a revolutionary discovery of the early twentieth century that changed our way of life forever. It has become an integral part of all consumer goods such as packaging, clothing, electronic devices, medicine, etc., (Andrady and Neal, 2009). However, high demand, massive production, extensive use, and poor plastic waste management contributes to plastic release and accumulation in the environment, which has become one of the most pressing environmental problems of our time (Geyer et al., 2017). Plastic waste accounts for 60 to 80% of all solid waste present in the aquatic environment (Gregory and Ryan, 1997), most of them being microplastics particles (MPs) (EPA US, 2016). MPs are plastic particles ranging in size from 1 µm to 5 mm (Horton et al., 2017), which are characterized by a variety of physical, chemical, and morphological properties such as different types of polymers and composition, size, shape, density, colour, etc. In the environment, MPs represent a group of persistent synthetic pollutants consisting of primary particles, manufactured at the millimetric or sub-millimetric scale under the form of pellets or microbeads, and secondary particles, resulting from the fragmentation of larger plastic debris through thermal, photo-oxidative, mechanical, and biological degradation processes (Cole et al., 2011). Because of their small size and ubiquitous distribution in all environmental compartments (Horton et al., 2017; Peng et al., 2020; Zhang et al., 2020), MPs are of great concern with respect to their bioavailability, toxicity and potential adverse effect on living organisms and ecosystem as a whole. Ingestion of MPs by aquatic living organisms from zooplankton (Cole et al., 2013) to mammals (Zantis et al., 2021), and the wide range of possible negative effects of plastic particles uptake are well documented. (EPA US, 2016; GESAMP, 2016; Peng et al., 2020).

However, there is a gap of knowledge on the interaction and the effects of MPs on the basic organisms of the trophic chain, such as microalgae, which are a major source of food for aquatic animals. Microalgae are photosynthetic microorganisms that are the most numerous primary producers in the entire aquatic ecosystem (Barbosa, 2009; Beardall and Raven, 2004). They are key organisms in a wide range of ecosystem functions, where they have an impact on ocean's carbon

sequestration (Singh and Ahluwalia, 2013), oxygen production, nutrient cycling, etc., (Hopes and Mock, 2015). Being ubiquitous, sensitive to environmental disturbances, and easy to cultivate in laboratory, microalgae are an ideal model to study the effects of different pollutants in the environment including MPs (Cid et al., 2012). The interaction between MPs and microalgae is a complex process that can lead to a multitude of effects acting on the further fate and behaviour of both MPs and microalgae, and thus potentially affecting the entire ecosystem (Nava and Leoni, 2021). For instance, in the environment, microalgae tend to colonize and form biofilms on abiotic surfaces (Irving and Allen, 2011), among them plastic surfaces, using them as an abiotic substrate to grow in a biofouling process (Bravo M et al., 2011; Carson et al., 2013; Jorissen, 2014; Reisser et al., 2014). While colonising plastic surfaces or other types of surfaces, microalgae cells secrete extracellular polymeric substances (EPS), which play an important role in biofilm formation. EPS consist of polysaccharides, lipids, nucleic acids, proteins, and other polymeric compounds (Wingender et al., 1999a; Xiao and Zheng, 2016), which favours cells cohesion and future adhesion to the substrate' surface (Wingender et al., 1999b). In addition, biofouling changes the density of plastic particles, affecting their buoyancy (Nava and Leoni, 2021; Oberbeckmann et al., 2015; Rummel et al., 2017) and thus leading to the dissemination of plastic particles through the water column by sinking to the bottom or moving to the surface. This widespread abundance of MPs particles consequently increases their bioavailability for various living organisms. Another effect of biofouling is a decrease in the hydrophobicity of the particle surface (Lobelle and Cunliffe, 2011). As a result, adsorption of toxic pollutants from the aquatic environment to the surface of the plastic particles can be enhanced (Bhagwat et al., 2021; Dong et al., 2017), which can amplify the toxicity of MPs. Moreover, extracellular polymeric substances (EPS) produced by microalgae promote the heteroaggregation of MPs and microalgae. The resulting aggregates become easy food for the aquatic organisms and are also more prone to sediment, thus here also affecting their dissemination through the water column as mentioned above (Lagarde et al., 2016; Long et al., 2015; Rummel et al., 2017). Then, MPs were also found to have a number of adverse effects on microalgae, including inhibition of growth

(Sjollema et al., 2016; Zhang et al., 2017; Liu et al., 2020; Song et al., 2020), decrease in chlorophyll content (Tunali et al., 2020; Wu et al., 2019) and photosynthetic activity (Zhang et al., 2017), physical and morphological damages (Mao et al., 2018), oxydative stress (Xiao et al., 2020). Finally, due to constant movement in the aquatic environment, plastic is a potential vector of geographic transport for the migration of microalgae (Rowenczyk et al., 2021). This phenomenon creates a risk of introducing pathogenic species (e.g. harmful algal blooms) into a new environment where native species are not adapted to defend themselves (Masó et al., 2003; Glibert *et al.*, 2014; Oberbeckmann et al., 2015).

For all these reasons, scientists are making increasing efforts to study the mechanism of MPs and microalgae interaction, to better understand its negative impact on a global scale. For instance, a recent review published by Nava *et al.* reports on the different effects that microplastics can have on microalgae cells. Their study shows that the effects on cell growth, photosynthesis and cell morphology are the most commonly reported effects, although this is highly dependent on both the type of plastic and the microalgae species considered. On the contrary, microalgae, by colonizing microplastics, also alter the plastic polymer, notably their density and sinking behaviour (Nava and Leoni, 2021). However, most of the ecotoxicological studies under laboratory conditions are using commercially manufactured models of MPs, in a vast majority of the studies the model plastic are polystyrene micro- or nano- spheres, which are not representative of plastic particles found in the environment (Gigault et al., 2021; Kokalj et al., 2021; Phuong et al., 2016). Thus, there is a need for research based on the use of an environmentally relevant model of plastic particles. For this purpose, we used a top-down method based on mechanical degradation to prepare more environmentally relevant model of MPs (Yakovenko et al., 2022). Particles were prepared from polyethylene as it is the most produced (Plastics Europe, 2020) and frequently found plastic type in the environment (Peng et al., 2020). The model particles were characterized by polydispersity, irregular shapes, and negative surface charge thereby representing several characteristics in common with the MPs formed in the environment. However, being small in size, these particles are hard to observe in the

biotic and abiotic matrices without destructive methods such as density separation or digestion. Thus, to overcome this limitation and make these particles easy to track and image in microalgae, we doped them by Lanthanide-based upconverting nanoparticles (UCNPs) as a luminescent tag. These recently developed phosphors are inorganic materials, very stable and able to convert low energy Near-Infrared photons into visible light (Gu and Zhang, 2018). This allows their detection even in thick samples such as in a tissue or a small animal. The studied model of MPs (Model-MPs) is represented by two types of particles: i) microparticles of PE itself (μ-PE); and ii) labelled microparticles of PE with UCNPs luminescence tag (μ-Upcon-PE).

In this study, we investigated the interaction between these Model-MPs and freshwater microalgae cells and their further role in the aggregation of cells using nano- and molecular scale experiments performed with an atomic force microscope (AFM) equipped with fluidic force microscopy (FluidFM). AFM, first developed in 1986 (Binnig et al., 1986), has proven over the years to be a powerful tool for surface characterization at the nanoscale (Pillet et al., 2014; Xiao and Dufrêne, 2016). In addition to high-resolution imaging capacities, down to the nanometer scale, AFM is also a sensitive force machine able to record piconewton level forces, thus making it possible to access the nanomechanical and adhesive properties of samples, as well as their interactions with their environment (Formosa-Dague et al., 2018). In the particular context of microalgae, AFM has been used to understand the morphology, nanostructure, nanomechanics and adhesive behavior of cells (Demir-Yilmaz et al., 2021), but most importantly their interactions with particles or molecules present in their environment (Besson et al., 2019; Demir et al., 2020; Demir-Yilmaz et al., 2021). In FluidFM, a microsized channel is integrated into an AFM cantilever and connected to a pressure controller, thus creating a continuous and closed fluidic conduit that can be filled with a solution or with air, while the tool can be immersed in a liquid environment (Meister et al., 2009). An aperture at the end of the cantilever allows air or the liquids inside the cantilever to be dispensed locally. In the first part of this study, Model-MPs were first characterized using AFM to visualize the particles and obtain information on their roughness. Then Fluidic force microscopy (FluidFM) was used to probe

their hydrophobic properties and probe their interaction with *Chlorella vulgaris* cells, a model green microalgae species. Finally, we describe these interactions by evaluating the possible contribution of EPS in the aggregation of cells.

2. Materials and Methods

2.1. Microalgae strain and culture.

The green freshwater microalgae *Chlorella vulgaris* strain CCAP 211/11B (Culture Collection of Algae and Protozoa) was cultivated in sterile conditions in Wright's cryptophyte (WC) medium prepared with deionized water (Guillard and Lorenzen, 1972). Cells were cultivated at 20°C, under 120 rpm agitation, in an incubator equipped with white neon light tubes providing illumination of approximately 40 µmol photons m^{-2} $s^{-1,}$ with a photoperiod of 18h light: 6h dark. All experiments were carried out with 7 days exponential phase batch cultures. Cells were first harvested by centrifugation (3000 rpm, 3 min at 21 °C), washed two times in phosphate buffered saline (PBS) at pH 7.4 and directly used for the AFM experiments and for some flocculation/flotation experiments (condition 3).

2.2. Microparticles model.

The synthesis and full characterization of the high-density polyethylene (HDPE) microparticle model, are described elsewhere (Yakovenko et al., 2022). Briefly, two bulk polymeric materials were prepared, including UCNPs-labelled HDPE (Upcon-PE) and UCNPs-free HDPE (Blank-PE). The oleate-capped NaREF4 (RE= rare earth, 2% Er; 30% Yb; 68% Y) with a diameter of 20 nm were used to provide a green luminescent plastic that can be directly observed by eye under 976 nm irradiation. UCNPs were incorporated into the HDPE (CAS 9002-88-4, Sigma Aldrich, Saint Louis, MO, USA) matrix by dissolving the polymer in boiling o-xylene (≥99.0% (GC grade); Sigma Aldrich, Saint Louis, MO, USA), containing UCNPs in a 10 wt.% HDPE:UCNPs ratio. The composite was separated from the reaction mixture by precipitation in the ice bath. The Blank-PE batch of polymer containing only

HDPE was prepared following the same protocol. Microparticles model was obtained by exposing each bulk material to a cryogenic grinder (SPEX™ SamplePrep 6775 Freezer/Mill™, Delta Labo, Avignon, France). The resulting polymer particles were dispersed in ethanol and fractionated by subsequent cascade filtration to micro- and nanosized particles. The collected microparticles were named as μ-PE (HDPE microparticles), and μ-Upcon-PE (HDPE labelled with the inclusion of UCNPs as a luminescent tag). The full characterization of the Model-MPs in terms of particle size, shape, crystallinity, chemical composition, surface charge, and luminescence properties, are described elsewhere (Yakovenko et al., 2022).

2.3. Zeta potential measurements.

Zeta-potential measurements for Model-MPs were carried out at 25°C on a Zetasizer Nano-ZS (Malvern Instruments, Ltd, UK) equipped with a He-Ne laser (λ = 633 nm) at an angle of 173°. Samples were prepared by dispersion of particles in 10 mM NaCl solution, to provide minimum level of conductivity in the samples, following ISO and ASTM standard guides (ASTM E2865-12, 2018). Before analysis, pH of every sample was measured. Zeta-potential and standard deviation (SD) were obtained from 5 measurements of 11 runs of 10 seconds using the Smoluchowski model (Yakovenko et al., 2022).

2.4. Model-MPs size measurements.

Size measurements for Model-MPs were carried out by Granulometry analysis using a Mastersizer MS3000 (Malvern Panalytical, UK) as described elsewhere (Yakovenko et al., 2022). Briefly, samples were prepared by dispersing the polymer powder in ethanol using HYDRO MV device with stirring at 2500 rpm. The refractive index used for ethanol and MPs were 1.36 and 1.52 respectively with an absorption index for particles of 0.1. Results are expressed as a percentage number. From these results, 90% of particles have a size below ± 15 μm, 50% of particles have size below ± 6 μm, and 10 % of particles have a size below ± 4μm. These are approximate average value obtained from the duplicates. The results are summarized in Table 1.

Table 1: *Summary of Model-MP characterization.*

Sample	Zeta potential, (mV)	Size distribution Dn (10)	Size distribution Dn (50)	Size distribution Dn (90)
µ-PE	-71 ± 7	4.3 ± 0.0	5.6 ± 0.1	11.9 ± 1.1
µ-Upcon-PE	-73 ± 8	4.12 ± 0.3	5.7 ± 0.5	13.25 ± 0.9

** 90%, 50% and 10% of the particles were observed to have sizes below the value given in the table.

2.5. Flocculation/flotation experiments.

To quantify the effects of Model-MPs on cell aggregation, flocculation/flotation separation of *C. vulgaris* was performed in dissolved air flotation (DAF) experiments in a homebuilt flotation device, shown in detail in Supplementary Figure S1. The depressurization at atmospheric pressure of water saturated by air at 6 bar induced the formation of bubbles. Water free of algae was pressurized for 30 min before injection into the jars. The injection was controlled by a solenoid valve and 20 mL of pressurized water was added to each beaker sample. Prior to bubble injection, cells were left to flocculate during 15 min. Flocculation/flotation tests were conducted in three different conditions, in each case in triplicate, with cells coming from 2 independent culture.

- **Condition 1:** *C. vulgaris* cells were cultured 7 days together with different concentrations of µ-PE and µ-Upcon-PE (final concentrations of 0, 5,10 and 40 mg/L for µ-PE and 40 mg/L for µ-Upcon-PE) until they reached mid-exponential phase. Then 100 mL of cell suspension was directly poured into the test-jars with an initial OD_{750} nm of 1.
- **Condition 2:** *C. vulgaris* cells were grown for 7 days until they reached mid-exponential phase. After that, 100 mL of cell suspension was directly poured into the test-jars with an initial OD_{750} nm of 1. Then µ-PE and µ-Upcon-PE were separately added (final concentration of 40 mg/L) to the suspension, which was stirred at 100 rpm for 15 min to homogenize it before introduction of the bubbles.

- **<u>Condition 3</u>:** *C. vulgaris* cells were grown for 7 days until they reached mid-exponential phase. After that, cells were harvested by centrifugation at 3000 rpm for 3 min, then washed twice with PBS buffer at pH 7.4. After that, 100 mL of cell suspension was directly poured into the test-jars with an initial OD_{750} nm of 1. Particles of µ-PE and µ-Upcon-PE were directly added (final concentration of 40 mg/L) to the suspension, which was stirred at 100 rpm for 15 min to homogenize it before introducing bubbles.

For all condition, after bubbles were introduced, the algal suspension was retrieved from the bottom of the test-jars: the first 5 mL of treated phase were discarded, the next 20 mL were used for quantifying flocculation/flotation efficiency. For that, the optical density of the withdrawn microalgae suspension was measured and compared to the optical density of the microalgae suspension measured before the experiments. The flotation efficiency (*E*) was calculated according to the following equation 1.

$$E = \frac{OD_i.V_i - OD_f.V_f}{OD_i.V_i} \quad (1)$$

2.6. Optical imaging experiments.

Flocculation was directly observed after resuspension of the cells in Phosphate Buffer Saline (PBS) at a pH 7.4 containing µ-PE or µ-Upcon-PE at a concentration of 40 mg/L. Flocculation levels were observed using an Axio Observer Z1 microscope (Zeiss, Germany) at high magnification (x50). To color EPS, an Alcian Blue staining was used as described previously (Vergnes et al., 2019). To this end, a solution containing Alcian blue at a final concentration of 0.018% and 0.036% of acetic acid solution was deposited on the glass surfaces where cells were immobilized and allowed to stand for 15 min. Glass surfaces were then immersed in distilled water for 5 min in order to remove the nonfixed staining. Finally, images were recorded at high magnification (×50) using an Axio Observer Z1 microscope (Zeiss, Germany).

2.7. AFM imaging.

For μ-PE and μ-Upcon-PE imaging, particles were immobilized on PDMS substrates. In each case at least 4 different particles were imaged in PBS at pH 7.4, using the Quantitative Imaging mode available on the Nanowizard III AFM (Bruker, USA), with MSCT cantilevers (Bruker, nominal spring constant of 0.01 N/m). Images were recorded with a resolution of 256 pixels × 256 pixels, at an applied force of <1.0 nN and a constant approach/retract speed of 90 μm/s (z-range of 3 μm). In all cases the cantilevers spring constants were determined by the thermal noise method prior to imaging (Hutter and Bechhoefer, 1993).

2.8. Roughness analyses.

Roughness analyses were performed on 9 different μ-PE and μ-Upcon-PE particles immobilized on PDMS and on 10 different *C. vulgaris* cells coming from at least 2 independent cultures after incubation with and without Model-MPs for 7 days, immobilized on positively charged glass slides (Superfrost™ Plus adhesion, Epredia, USA). Individual μ-PE and μ-Upcon-PE images were recorded in PBS whereas for cells, after incubation with Model-MPs, samples were directly imaged in culture medium using contact mode with a Nanowizard III AFM (Bruker, USA), using MSCT cantilevers (Bruker, nominal spring constant of 0.01 N/m). Images were recorded in contact mode using an applied force of < 1 nN for micro-HDPE-(UCNPs) and of < 0.5 for cells and the cantilever spring constants were determined by the thermal noise method prior to imaging (Hutter and Bechhoefer, 1993).

2.9. Hydrophobicity measurements.

To measure the hydrophobic properties of materials, a recently developed method was used, which consists in measuring using Fluidic force microscopy (FluidFM), the interactions between a bubble (hydrophobic surface) and materials (Demir et al., 2021). For that, FluidFM probes with an aperture of 8 μm of diameter (Cytosurge AG, Switzerland) were hydrophobized by coating with self-assembled monolayers (SAMs) of silanes via SAMs vapor deposition technique. FluidFM cantilevers were functionalized with 1H,1H,2H,2H-Perfluorodecyltrichlorosilane (FDTS) using an Orbis-1000

equipment (Memsstar, Livingston, UK) to make their external surface and inside microchannel hydrophobic. The deposition was realized under vacuum at 40 torrs and -40°C, for 5 min. Then the microchannel of these silanized cantilevers was filled with air and the probe was immersed in PBS 1X. To eliminate any particle or dust contamination or to prevent clogging of the FluidFM cantilever, a slight over pressure of 20 mbar was applied. Then to produce a bubble at the aperture of the cantilever, a positive pressure of 200 mbar was applied inside the microfluidic cantilever in buffer. The silanized probes were calibrated using the thermal noise method before each measurement (Hutter and Bechhoefer, 1993). The interactions between the bubbles produced and MPs were then recorded in force spectroscopy mode using a maximum applied force of 2 nN, a constant approach retraction speed of 3 µm/s, and a delay time of 1.0 s. For each conditions, areas of 0.5 x 0.5 µm on 5 different MPs were probed. Adhesion forces were obtained by calculating the maximum adhesion force on the retract force curves obtained; data are presented in Supplementary Table 1-3.

2.10. Force spectroscopy experiments using FluidFM technology.

Force spectroscopy experiments were conducted using a NanoWizard III AFM (Bruker, USA), equipped with FluidFM technology (Cytosurge AG, Switzerland). In each case, experiments were performed in PBS, using micropipette probes with an aperture of 2 µm (spring constant of 0.3, and 4 N/m, Cytosurge AG, Switzerland). First, PBS at a pH of 7.4 was used to fill the probe reservoir (5 µL); by applying an overpressure (100 mBar) the PBS then filled the entire cantilever microchannel. The probe was then immersed in PBS and calibrated using the thermal noise method prior to measurement (Hutter and Bechhoefer, 1993). A single *C. vulgaris* cell was then aspirated from the surface of the Petri dish by approaching the FluidFM probe and applying a negative pressure (−200 mBar). The presence of the cell on the probe was verified by optical microscopy. The cell probe was then used to measure the interactions with Model-MPs. For that, µ-PE and µ-Upcon-PE solutions at a concentration of 40 mg/L were deposited on polydimethylsiloxane (PDMS) surfaces and left for 30 min. After that, the PDMS surfaces were rinsed using PBS and directly used. Interactions between single *C. vulgaris* cells aspirated at the aperture of FluidFM cantilevers and Model-MPs were

recorded at a constant applied force of 2 nN, force curves were recorded with a z-range of up to 2 µm and a constant retraction speed of 2.0 µm/s to 20 µm/s. In each case, at least 6 cells coming from 2 independent culture were probed. Data were analyzed using the Data Processing software from Bruker; they are presented in Supplementary Tables 4-6. Adhesion forces were obtained by calculating the maximum adhesion force for each retract curves. Experiments were repeated three times with ten different cells coming from at least three different cultures.

2.11. Two-photon microscopy.

Samples were imaged on a Zeiss LSM-710 two-photon microscope, equipped with a Ti: Sapphire Chameleon Vision II laser (Coherent, Santa Clara, California), operating at 980 nm (2-3% of max power for UCNPs and 50% for *C. vulgaris* and µ-Upcon-PE samples, 140 fs pulses, 80 MHz repetition rate), and a Zeiss Plan-Apochromat 63x/1.40 oil immersion lens. Upconverted light was collected between 490 and 600 nm for the green band, and 630 and 710 nm for the red band. Emission spectrum of analyzed samples were collected between 418 and 729nm with a 10 nm step. Images were processed using ImageJ (Fiji) software (Yakovenko et al., 2022).

2.11 Statistical analysis.

Experimental results represent the mean ± standard deviation (SD) of at least three replicates. For each experiments, the number of replicates is indicated both in the Material and Methods section in the corresponding paragraphs, and in the Results and Discussion section. For large samples ($n>20$ values) unpaired student t-test was used to evaluate if the differences between the conditions are significant. For small samples ($n<20$ values) non-parametric Mann and Whitney test was used to assess the differences. The differences were considered significant at $p<0.05$.

3. Results and discussion

3.1. Model-MPs are irregular, have a rough surface and hydrophobic properties

The Model-MPs were derived from previous work (Yakovenko et al., 2022), where they were prepared from raw commercially available high-density polyethylene (PE). The top-down method consisted in the cryogenic grinding of the polymer or the nanocomposite (PE loaded with 10% UCNPs by high temperature swelling in xylene). This method is interesting because grinding is achieved at a temperature below the vitreous transition of PE and elastic substances are generally then more easily processed. The grinding at this temperature also prevents the chemical alteration of the PE backbone (this was ensured by infrared measurements) or morphological modification (calorimetric experiments) (Yakovenko et al., 2022). The size distribution of the particles obtained by granulometric analysis showed that around 90% of the particles in number were smaller than 15 µm. These Model-MPs (both µ-PE and µ-Upcon-PE) were first characterized using AFM in contact mode. The images obtained are presented in Figure 1. The 3D AFM height images (Figure 1a and b) and vertical deflection (Figure 1c and d) images recorded show that both types of Model-MPs have an irregular shape and a heterogeneous surface, like microplastics collected in the environment (ter Halle et al., 2016). In addition, they are found mostly aggregated on top of each other, and not present as single isolated particles. This is illustrated by the cross-section taken along the longer sides of the particles in Figure 2c and d, which clearly show this irregularity, with height variations over 6 nm in Figure 1e and f. This tendency of Model-MPs to form aggregates could be explained by their hydrophobicity. Such behaviour is not observed with model plastic micro- and nanospheres commercially available, which are formulated with different surfactant additives allowing to prevent this aggregation. However, these models are not reliable because their chemical properties and further interactions are different from the plastic particles found in the environment (Phuong et al., 2016).

We then acquired high resolution images on small areas (5µm $\times$ 5µm) on top of the particles, using advanced quantitative imaging (QI) mode; the resulting images are shown in Figure 1g-h. In this case, QI mode was used instead of contact mode because of the complexity of Model-MPs surfaces. QI being a force spectroscopy based imaging mode, there is no lateral forces exerted by the tip as

occurring in contact mode, which can damage the sample (Chopinet et al., 2013). This way we could obtain high-resolution images of the particles surface (Figure 1i and j), and quantify their roughness. Roughness measurements were performed on 9 different particles for both type of Model-MPs (µPE and µ-Upcon-PE); the results of these analysis are presented in the boxplot Figure 1k. They show that µ-PE have an average roughness of 3.7 ± 1.1 nm, which increases to 7.6 ± 5.4 nm when UCNPs are incorporated in the particles (µ-Upcon-PE). Although there is an important heterogeneity in the measurements in this last case, the difference with the µ-PE is not significantly different at 0.05 level (non-parametric Mann and Whitney test). This result thus shows that the incorporation of UCNPs may affect the structure of Model-MPs, by modifying their surface morphology; however, the heterogeneity of the measurements performed on µ-Upcon-PE reflects the uncontrolled incorporation of the UCNPs over the particles present in the sample (Yakovenko et al., 2022). The surface roughness of particles is an important physical characteristic that plays a major role in how they will behave in the environment and interact with microorganisms. Commercially available models of micro- and nanospheres used for ecotoxicological studies are usually characterized by a very smooth surface (Phuong et al., 2016; Rubin et al., 2021), whereas plastic particles found in the environment are characterized by a rough surface (Rowenczyk et al., 2020). Thus, our Model-MPs, which have a high average surface roughness, can be considered as a more reliable model to study the interactions between MPs and microorganisms such as *C. vulgaris.*

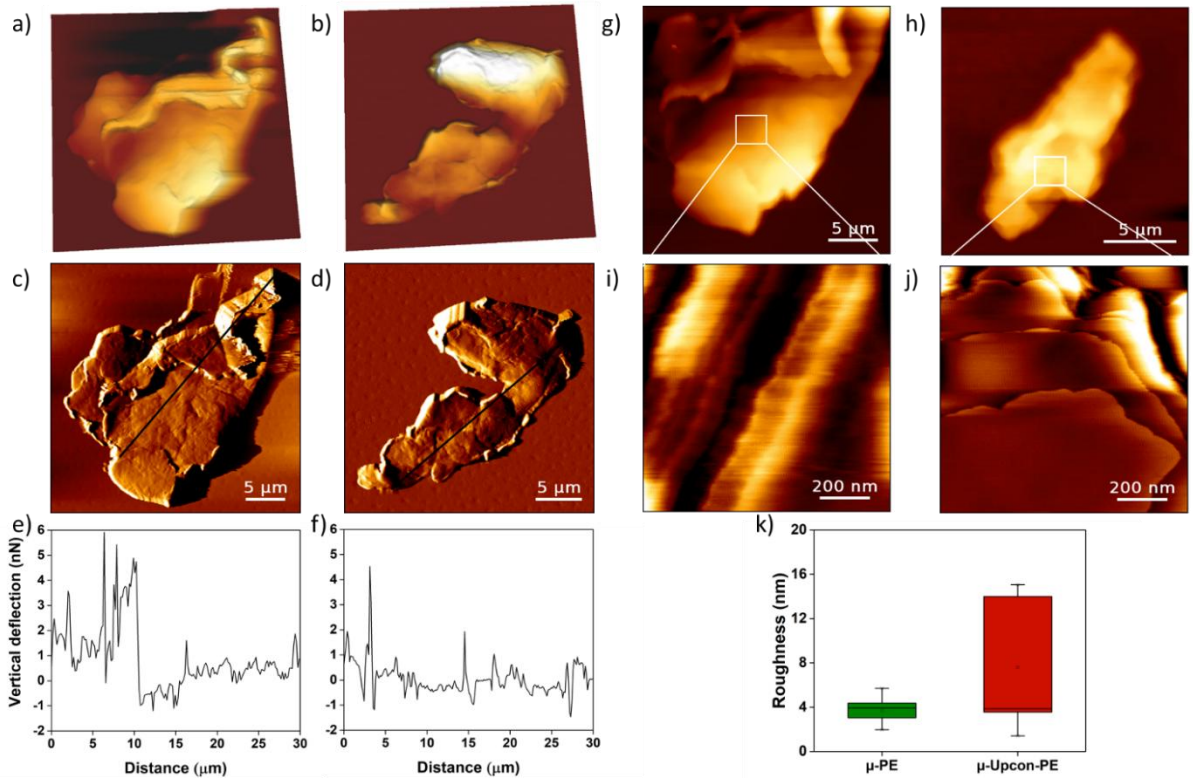

Figure 1: Imaging and characterization of µ-PE surface before and after incorporation of UCNPs: *a) 3D AFM height image of µ-PE (color scale = 7 µm); b) 3D AFM height image of µ-Upcon-PE (color scale = 4 µm); c) Vertical deflection images of µ-PE; d) Vertical deflection images of µ-Upcon-PE; e) Cross section taken along the larger side in panel c and f) Cross section taken along the larger side in panel d; g) AFM height images of µ-PE (color scale = 7 µm) and h) AFM height images of µ-Upcon-PE (color scale = 5 µm); i) AFM height images of µ-PE surface (5µm × 5µm) (color scale = 23 nm) and j) AFM height images of µ-Upcon-PE surface (5µm × 5µm) (color scale = 19 nm); k) Quantification of µ-PE and µ-Upcon-PE surface roughness in a box plot.*

In the next step we then assessed the hydrophobic properties of the Model-MPs, which are an important physico-chemical factor that could greatly influence their interactions with microalgae. To this end, we used a recently developed method that consists in probing the interactions of samples with bubbles produced using FluidFM technology (Demir et al., 2021), which combines AFM with microfluidics (Meister et al., 2009). Air bubbles in water behave like hydrophobic surfaces. By producing them using FluidFM, it is then possible to probe their interactions with complex abiotic surfaces such as the MPs, and to measure their hydrophobic properties with accuracy. Such

measurements allow avoiding usual issues related to other tests like water contact angle measurement (WCA). To perform these experiments, Model-MPs were immobilized on a PDMS substrate and their interactions with bubbles were measured in PBS buffer at pH 7.4 (Figure 2a). For both µ-PE and µ-Upcon-PE, 5 different particles were probed. In the case of µ-PE, the retract force curves obtained (inset in Figure 2a) show a single peak occurring at the contact point, typical of a hydrophobic interaction (Dague et al., 2007), with an average force of 10.1 ± 6.2 nN (Figure 2a, n= 2558 force curves obtained from 5 different particles, adhesion values can be found in Supplementary Table 1). This force corresponds to the height of the adhesion peak, and thus to the force needed to break the interaction between the bubble and the sample. As a hydrophobic interface like bubbles interact with hydrophobic surfaces, then this force reflects the degree of hydrophobicity of the sample, the stronger the adhesion, the higher the hydrophobicity. Similarly, in the case of µ-Upcon-PE, a single peak occurring at the contact point is visible (inset in Figure 2b); retract adhesion forces in this case were on average of 13.7 ± 15.3 nN (Figure 2b, n = 2107 force curves obtained from 5 different particles, adhesion values can be found in Supplementary Table 2). The large distribution of the adhesion values obtained in these experiments reflect the irregularities of the Model-MPs used that were visible on the height AFM images in terms of nanostructure. Indeed, in each case these irregularities change the contact area between the bubble and the particle, which can have an impact on the adhesion force value recorded. Thus in conclusion the two samples (µ-PE and µ-Upcon-PE) present hydrophobic properties as they are able to interact with bubbles with a relatively important force (for comparison, the interaction between *C. vulgaris* cell surface and bubbles give an average adhesion force of 4.2 nN, Demir et al., 2021). Plastic particles found in the environment probably have more hydrophilic properties, caused by plastic aging and oxidation (Liu et al., 2021). Thus the Model-MPs used in this study are a relevant model of plastic that has just entered the environment, prior to the oxidation process.

The experiments were then repeated with Model-MPs that were incubated with cells during their culture (7 days, Figure 2c). In this case also, hydrophobic interactions are recorded, with an

409 average adhesion force of 16.4 ± 8.0 nN (n= 1685 force curves obtained from 5 different particles,
410 adhesion values can be found in Supplementary Table 3), a value that is significantly different from
411 the two first conditions (p-value of 0.05, unpaired student test). Thus, the incubation of Model-MPs
412 with cells changes their hydrophobic properties. This is an important point because it means that our
413 Model-MPs, after seven days exposed to the cells, have their surface modified; a plausible hypothesis
414 could be that cells produce EPS in the culture medium, which then could coat the particles surface.
415 Finally, in order to confirm that the forces recorded are due only to the interactions between Model-
416 MPs and bubbles, we also probed the interactions between bubbles and the PDMS surfaces used to
417 immobilize the particles. The results presented in Supplementary Figure S2 show an average
418 adhesion force recorded of 1500 ± 100 nN (n = 2500 force curves). This adhesion force is much
419 higher than the ones obtained with Model-MPs (maximum around 50 nN), thus meaning that we
420 could precisely measure the interaction between bubbles and the particles without interfering with
421 the surface on which they are immobilized. In the natural environment, microplastics undergo
422 alterations, including among multiple factors, oxidation of the polymer that changes its polarity and
423 possibly its hydrophobicity (Andrady et al., 2011). FTIR analysis performed on the synthetized particle
424 did not show any oxidation bands (Yakovenko et al., 2022). However, Model-MPs have a negative
425 zeta potential and FTIR is most likely not sensitive enough to detect these functionalities if they are
426 present in small proportions. Small microplastics and nanoplastic are expected to be negatively
427 charged (Gigault et al., 2021). Because the particles synthesized here are also negatively charged,
428 they have supposedly a similar behaviour than weathered plastic particles. Thus, altogether the
429 biophysical characterization of the Model-MPs produced in this study show that they are aggregated,
430 have a rough surface and present hydrophobic properties. MPs found in the environment have
431 similar characteristics (Phuong et al., 2016), thus confirming the interest of our methodology to
432 obtain particles close to what can be found in the environment. Our Model-MPs are thus a reliable
433 model to understand the interactions that MPs can have with microalgae in the environment.

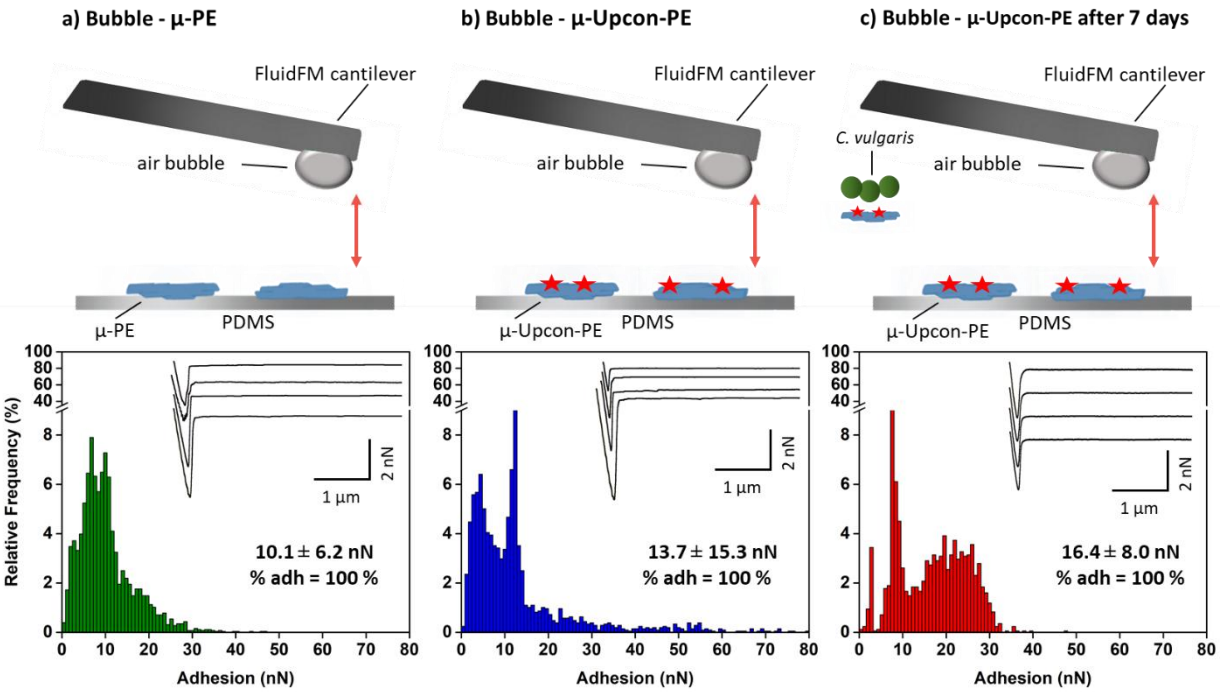

434 ***Figure 2: Probing the interaction between bubble and Model-MPs:*** *Adhesion force histogram*
435 *obtained for the interaction between bubbles and a) µ-PE, b) µ-Upcon-PE, and c) µ-Upcon-PE after*
436 *incubation for 7 days with C. vulgaris cells. Insets in a, b and c shows the representative force curves*
437 *obtained during force spectroscopy experiments.*

438 **3.2. Model-MPs do not affect cell growth or morphology but have an effect on their aggregation.**

439 In a second part of the study, we evaluated the effects of Model-MPs on cell growth. In the
440 literature, studies state that PS MPs of 100 µm have no toxic effect up to 50 mg/L (Yan et al., 2021),
441 the same was reported for MPs of 1-5 µm, which had no effect on microalgae up to 41.5 mg/L (Prata
442 et al., 2018). To verify whether it is the case for our Model-MPs and our microalgae strain, we
443 monitored the cell growth of *C. vulgaris*, incubated or not with Model-MPs at a concentration of 40
444 mg/L, which is the maximum concentration that we will use throughout this study. This
445 concentration is most likely higher than the exposure concentrations encountered in the
446 environment, however it allows us to observe and further characterize the effects on microalgae
447 cells, which could not be detected otherwise. In addition, for small microplastics like the ones used in
448 this study (5 µm), no data on their environmental concentrations are provided in the literature, as
449 most studies report data for particles between 300 µm and 5 mm. It is thus difficult to predict the

concentrations of small particles in a natural sample. The growth curves obtained are presented in Figure 3a; they show that in each case cell growth is similar, thereby showing that neither µ-PE nor µ-Upcon-PE affect *C. vulgaris* cell growth. This is in good agreement with the data from the literature although the type of plastic used was not the same. In addition, this also shows that UCNPs are not toxic, as µ-Upcon-PE do not have an effect on cell growth. Moreover, incubation with Model-MPs do not extend the exponential phase, meaning that *C. vulgaris* cells and Model-MPs do not have a symbiotic relation either, as it was shown for other species. Indeed, Kang *et al.* observed that organic intermediates resulting from MPs degradation can serve as a carbon source for algae (Kang et al., 2019). Also in some cases, cell growth can be modified resulting from the EPS production (Casabianca et al., 2020; Cunha et al., 2019; Long et al., 2017), but this is not the case here.

We then went down to the nanometer scale to evaluate if the presence of Model-MPs in the culture medium had an effect on cell surface structure. For that, we incubated *C. vulgaris* during 7 days together with µ-PE, and took a close look at the cell surface and measured the roughness on small areas (0.3 µm × 0.3 µm) on top of the cells in contact mode, as shown in Figure 3b and c in normal conditions or incubated with µ-PE for 7 days, respectively. These measurements were repeated on 10 different *C. vulgaris* cells coming from at least 2 independent cultures in each case; the results of these analysis are presented in the boxplot Figure 3d. They show that *C. vulgaris* cells have an average roughness of 0.8 ± 0.2 nm, which stays similar, of 0.6 ± 0.2 nm, when cells are incubated with µ-PE. Cell wall roughness of *C. vulgaris* was determined before at different pH values (6 and 8) using AFM in a study by Demir *et al.* (Demir et al., 2020) and were in the same range. Overall, these data show that the Model-MPs used at concentrations up to 40 mg/L have no effect on either cell growth or cell nanostructure after 7 days of co-incubation.

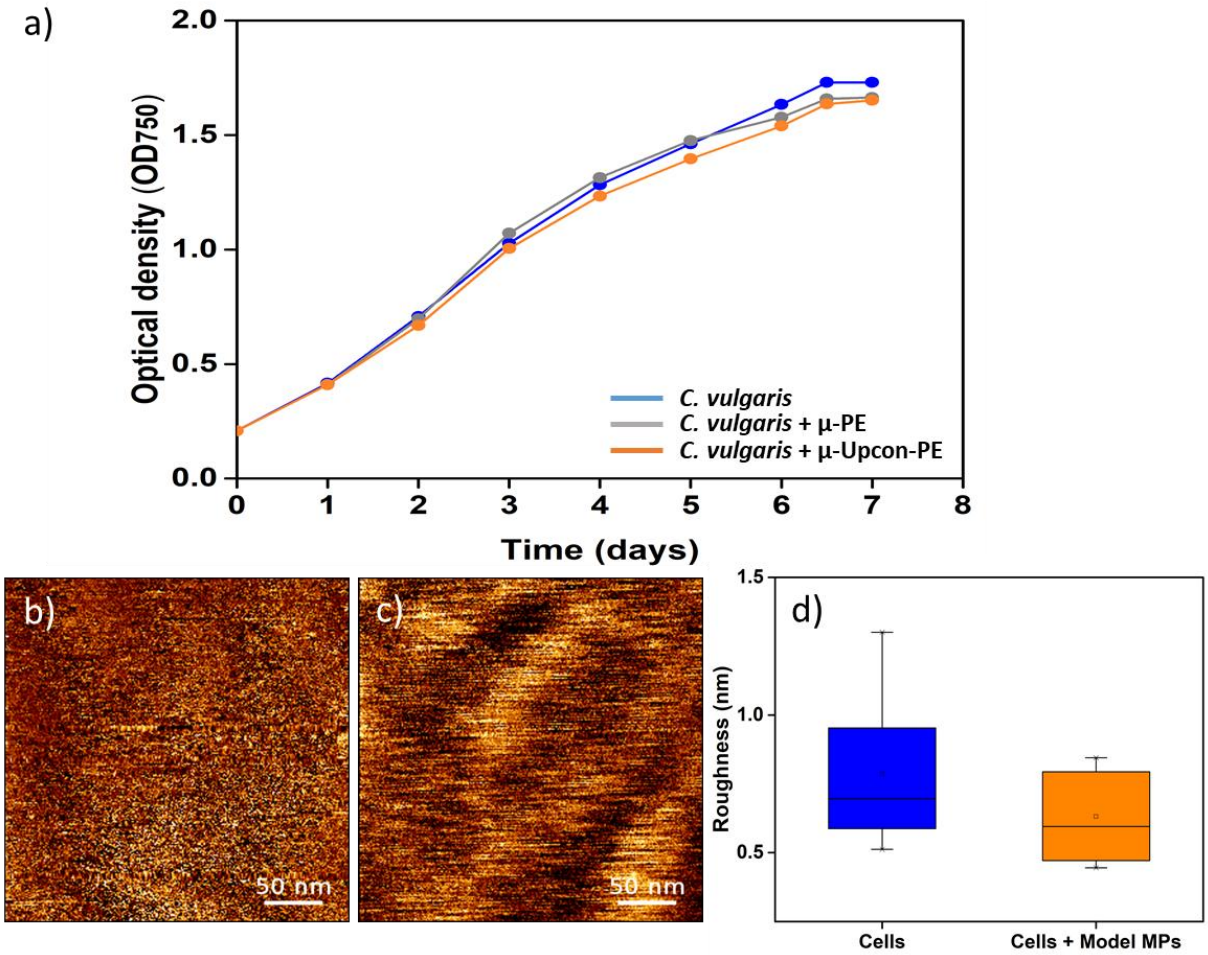

472 ***Figure 3: Characterization of C. vulgaris cells in interaction with Model-MPs.*** *a) Variations in optical*
473 *density of C. vulgaris cells before and after incubated with Model-MPs (µ-PE and µ-Upcon-PE); b) AFM*
474 *height images of C. vulgaris cell surface (0.3 µm × 0.3 µm) in contact mode (color scale = 6 nm) and c)*
475 *AFM height images of C. vulgaris cell surface (0.3 µm × 0.3 µm) after incubated 7 days together with*
476 *Model-MPs in contact mode (color scale = 8 nm); d) Quantification roughness values of C. vulgaris cell*
477 *before and after incubation with Model-MPs for 7 days in a box plot.*

478

479 Although our Model-MPs do not have an effect on *C. vulgaris* cell growth or cell

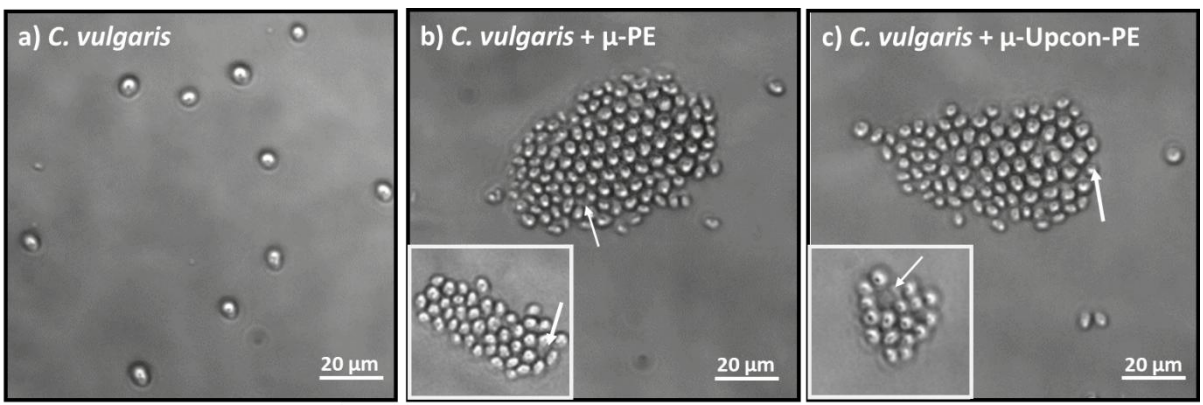

nanostructure, their addition to the culture medium could have an influence on the cell aggregation. To evaluate this, we performed both optical microscopy imaging (Figure 4a-c) and two-photon microscopy imaging (Figure 4d-f). In these experiments, cells were incubated 7 days with µ-PE and µ-Upcon-PE at the concentration of 40 mg/L. In the control condition (Figure 4a, without Model-MPs), we can see that cells are randomly distributed over the surface and no cell aggregation is observed. In the cases cells were incubated with µ-PE and µ-Upcon-PE (Figure 4b and c), large aggregates of cells are visible around what seems to be Model-MPs particles, indicated by the arrows on the images.

Figure 4: Images of C. vulgaris cells. *Bright field images of cells after incubated 7 days with: a) nothing; b) µ-PE; c) µ-Upcon-PE. The arrow indicated the Model-MPs.*

Thus, these first images suggest that Model-MPs cause the aggregation of cells. However, because of the small size of Model-MPs, it is difficult to identify them with certainty and understand their real implication in cell aggregation. In a next experiment, we thus took advantage of the luminescence properties of µ-Upcon-PE, and made observations of cells incubated with µ-Upcon-PE for 7 days (concentration 40mg/L) using a two-photon scanning microscope under an excitation at 980 nm (Yakovenko et al., 2022). On the bright field image (Figure 5a) big aggregate of cells can be observed as well as what we expect to be µ-Upcon-PE particles. The composition of these aggregates was confirmed by the green (Figure 5b) and red (Figure 5c) emissions under NIR irradiation. In the case of µ-Upcon-PE, this emission corresponds to strong sharp green (515-575 nm) and red (630-680 nm) emission bands characteristic for Er-based UCNPs incorporated into µ-Upcon-PE, as visible on the emission spectra in Figure 5d. *C. vulgaris* cells are characterized by a weak autofluorescence (Takahashi, 2019; Tang and Dobbs, 2007), also visible on the spectra in Figure 5d. Upconversion and autofluorescence spectra could be easily unmixed thanks to the limited spectra overlap especially in the green, and the discrepancy in signal intensity (varying from different order of magnitude) between upconversion and 2-photon emission (Figure 5d). Brightfield as well as bi-photon images of

UCNPs alone, µ-Upcon-PE alone and *C. vulgaris* cells alone can be found in Supplementary Figure S3. These results allow us not only to accurately determine the presence and location of µ-Upcon-PE in cell aggregates, but also to show two different things: i) the µ-Upcon-PE are in fact distributed over a large part of the aggregate, which could not be visible on the standard optical microscopy images, and ii) some cells are not directly bound to the particles (cells in the bottom-left part on the image 5d-f), which suggest that perhaps the aggregation in the presence of Model-MPs can occur through a different mechanism than direct binding.

Figure 5: *Two-photon microscopy imaging of µ-Upcon-PE and C. vulgaris aggregate after 7 days inoculation together: a) Brightfield image; b) Green emission under NIR irradiation and c) red emission under NIR irradiation observed for µ-Upcon-PE and C. vulgaris aggregate. Images show Z-*

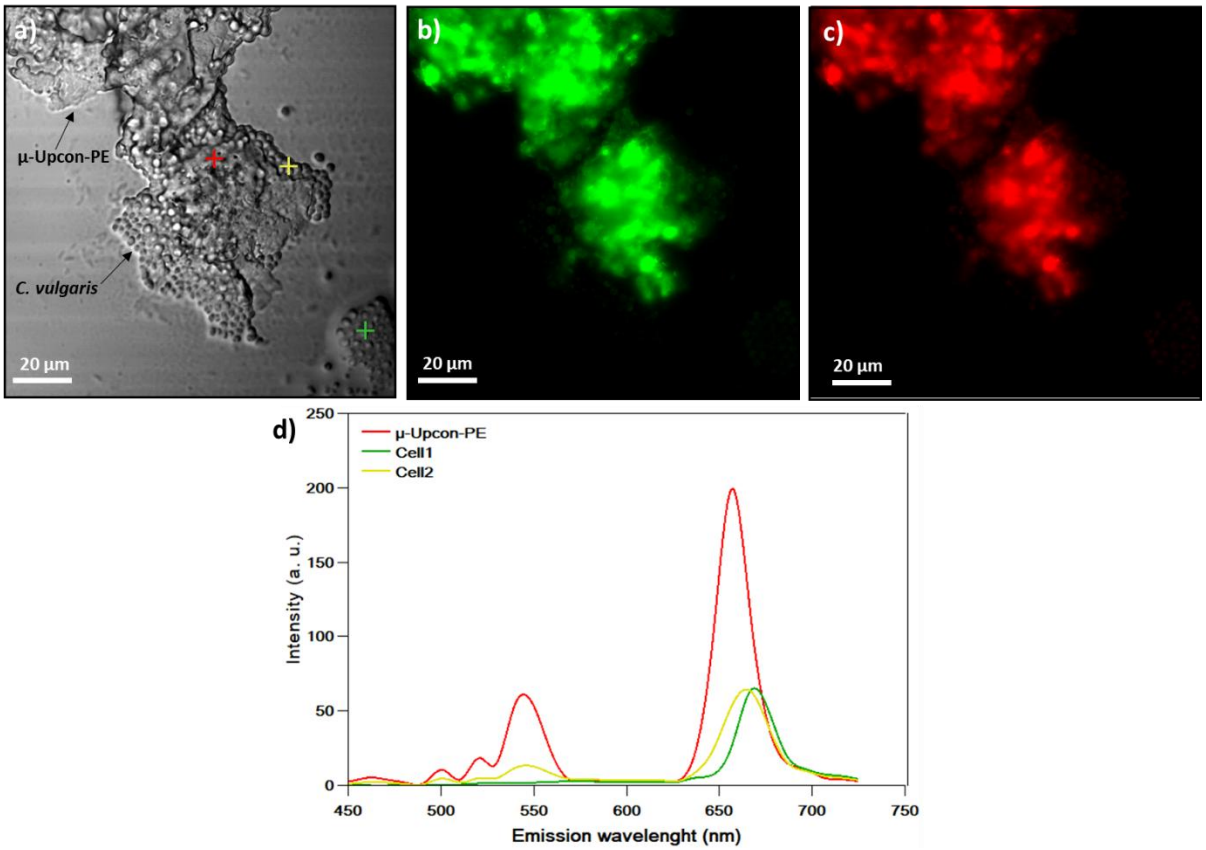

projection in a maximum intensity. d) Upconversion emission spectra of µ-Upcon-PE together with two-photon emission spectra of C. vulgaris cells. The positions where the spectra were recorded on the image is indicated by the coloured crosses on a).

Because these observations are qualitative, we then looked for a way to quantify the effect of Model-MPs on cell aggregation, and performed flocculation/flotation experiments with different µ-PE concentrations (final concentration of 0, 5, 10 and 40 mg/L) incubated 7 days together with *C. vulgaris* cells. The results are presented in Supplementary Figure S4. In such experiments, cells can be separated from the water by bubbles only if they are aggregated into flocs that are easily captured by the rising bubbles and carried to the surface. The flotation step allows separating the aggregated cells from the suspension, and thus to quantify the influence of Model-MPs on cell aggregation, which is reflected by the separation efficiency percentage. In this case using bubbles was more efficient than leaving the flocs to settle down because of their small size and low density. In the absence of Model-MPs, the separation efficiency obtained is of 16 ± 5 %; this number reflects the natural flocculation taking place in 7 days old-cultures, which is often the result of the natural production of EPS by cells (Vergnes et al., 2019). When adding Model-MPs at a concentration of 5 mg/L and 10 mg/L into the culture medium for the 7 days of the culture, the separation efficiencies are even lower, indicating that in these cases the addition of the MPs do not trigger any flocculation. This is an interesting point because it means that to obtain aggregation, the concentration of MPs must be important in the environment. Finally, as we expected from the optical microscopy experiments, when cells are incubated with Model-MPs at a concentration of 40 mg/L, the separation efficiency increases significantly, to around 50%, indicating that cell aggregation occurs, but does not reach the entire cell suspension. Different hypotheses could explain the fact that at this concentration only, cell aggregation occurs. The principal one could be that the presence of a certain concentration of Model-MPs in the medium during culture triggers the production of EPS, which can flocculate cells, as it has already been showed in the literature (Harrison et al., 2014; Lagarde et al., 2016; Yan et al., 2021).

To test this hypothesis, flocculation/flotation experiments were repeated at 40 mg/L concentration in different conditions (Figure 6). In the first condition, Model-MPs were incubated for 7 days together with *C. vulgaris* cells before conducting the experiments. In the second condition, the

cells in culture were not exposed to the Model-MPs, instead particles were added at the end of the culture, for 15 minutes before flocculation/flotation experiments. The comparison of the results obtained in these two conditions will help understanding if and how EPS interacts with Model-MPs, or if cells produce more EPS when they are cultured in the presence of these particles. Finally in the third condition, at the end of the cultures cells were washed in PBS to remove the EPS they may have produced, and then only Model-MPs were added for 15 minutes before flocculation/flotation experiments. The results obtained in each case are presented in Figure 6, they show that there is no significant difference between condition 1 (flocculation efficiency of 51 ± 11% for μ-Upcon-PE) and condition 2 (flocculation efficiency of 61 ± 4% for μ-Upcon-PE), meaning that even if cells are not grown in the presence of Model-MPs, cell aggregation can still occur, and takes place rapidly as 15 minutes only are sufficient to obtain a separation efficiency similar to the one obtained in condition 1. An important point to note is that the modification of the Model-MPs used with UCNPs does not have an effect on the flocculation/flotation efficiency, as similar efficiencies are observed with both types of microparticles (μ-PE and μ-Upcon-PE). In condition 3, when EPS are removed from the cells by centrifugation, the separation efficiency stays similar when μ-PE are used (flocculation efficiency of 47 ± 19% for μ -PE), and decreases to 18 ± 19% when μ-Upcon-PE are used. Note that in this case, the standard deviations obtained are large; non-parametric statistical test (Mann and Whitney test) showed that the differences with condition 1 and condition 2 are in fact not significant when both samples are used (μ-PE and μ-Upcon-PE). But still, these large standard deviations obtained in conditions 3, even if the differences are not significant, tend to suggest that EPS could be involved in the aggregation of cells, which may interact with MPs when they are added to the culture media.

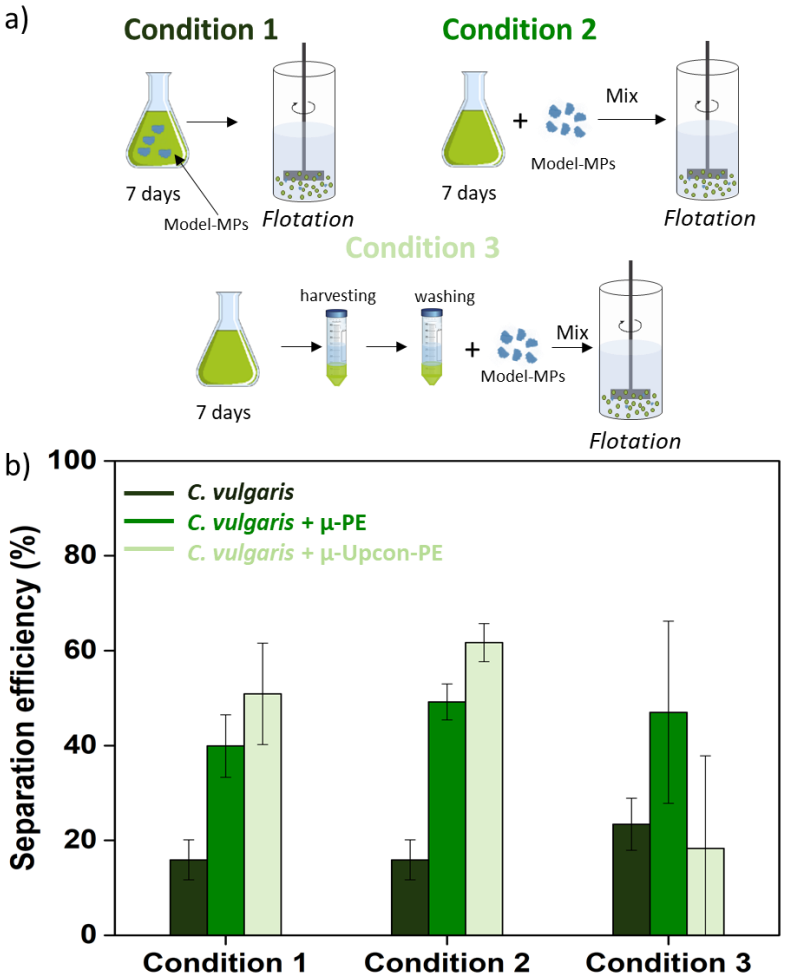

Figure 6: Flocculation experiments of C. vulgaris. *a) Schematic representation of the conditions used for flotation/flocculation experiments. Condition 1: Model-MPs + cells after 7 days incubation together (no washing). Condition 2: Model-MPs are directly added to cells (no washing). Condition 3: Model-MPs are directly added to cells (washing PBS). b) C. vulgaris cell separation efficiency with Model-MPs (µ-PE and µ-Upcon-PE) at 40 mg/L concentration under the different conditions described in a).*

3.3. Model-MPs induced aggregation can take place through different mechanisms

To understand if the presence of EPS is an important factor or not in the aggregation of cells in the presence of Model-MPs, we performed additional optical microscopy assays using Alcian blue staining. This dye is known to react specifically with acidic polysaccharides (Reddy et al., 1996; Shiraishi, 2015; Vergnes et al., 2019) present in the EPS excreted by microalgae cells, thus we selected this technique to qualitatively evaluate the presence of EPS excreted by cells grown in

presence of Model-MPs. The images obtained are presented in Figure 7. They show that when cells are grown without Model-MPs (Figure 7a), cells produce EPS in a small amount. In particular, we can see here the presence of small cell aggregates that are entrapped with the EPS visible on the image (Figure 7a). This is in line with the flocculation/flotation results obtained that shows that cells without MPs can still be separated with an efficiency of 16% (Supplementary Figure S3). When cells have grown for 7 days in the presence of Model-MPs, large aggregates of cells are visible on the images, on which large amounts of EPS can be observed (Figure 7b and c). These observations thus suggest that the presence of Model-MPs in the culture medium triggers the production of EPS, as the cells use them as a support to form biofilms around them (Yan et al., 2021), which is in line with the previous literature on this subject (Harrison et al., 2014; Lagarde et al., 2016; Yan et al., 2021). When we put these observations in perspective with the flocculation/flotation tests performed before, it seems that the separation efficiency that we obtain when cells have been grown for 7 days with the MPs is due to the increased production of EPS by the cells in a biofouling process. However, the direct interaction of Model-MPs with cells seem also to induce aggregation (Figure 6 condition 2); as it can be seen on these images (Figure 7b and c), cells do produce some EPS even if not grown with MPs, and the decreasing trend of the separation efficiency obtained when cells are washed before flocculation/flotation experiments (Figure 6, condition 3) would suggest that MPs can interact directly with these EPS. The fact that the separations efficiencies when cells washed are not significantly different could also suggest that this interaction could also be in part directly the cell wall of cells. Another interesting point is that when cells have been grown with MPs, a certain concentration is needed to induce cell aggregation: in this case this would mean that both the production of EPS and the aggregation induced by contact between MPs and cells is concentration dependent. When there are not enough MPs in the medium, the surface area of flocculant (MPs) could be too small compared to the surface area of cells to aggregate them.

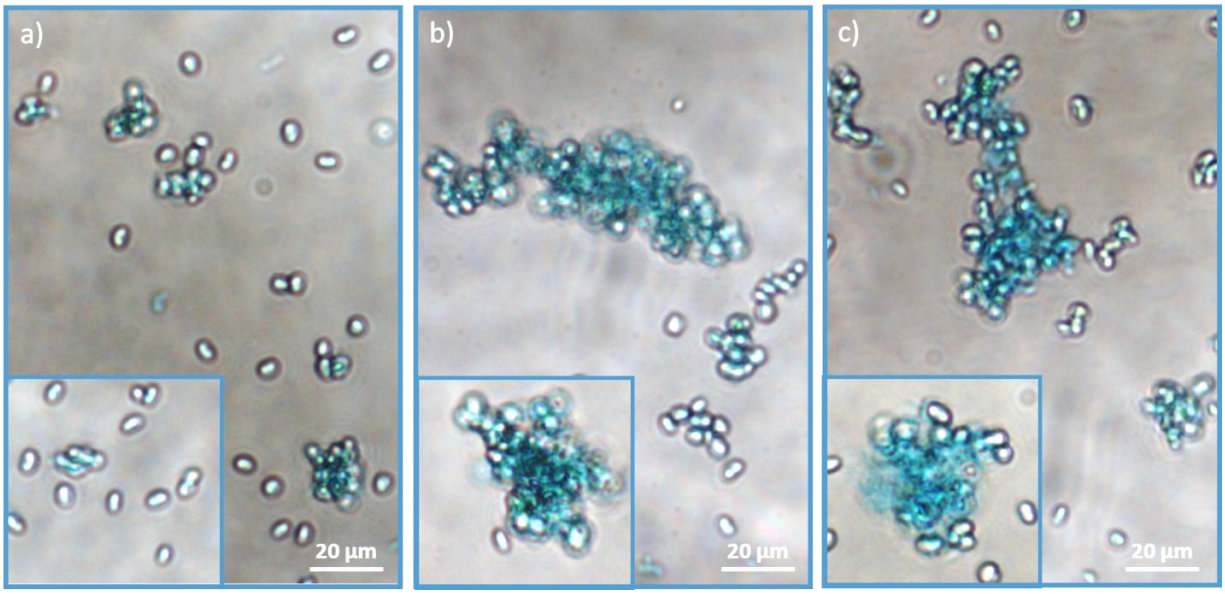

Figure 7. Staining EPS produced by C. vulgaris with Alcian blue. *Optical images of cells dyed with Alcian blue, a) grown in normal conditions for 7 days, b) grown in the presence of 40 mg/L of µ-PE during 7 days, and c) grown in the presence of 40 mg/L of µ-Upcon-PE during 7 days.*

While these results together bring explanations on the mechanism by which Model-MPs induce the aggregation of cells, a final point needs to be clarified; are the Model-MPs able to directly interact with cells? This would allow understanding why cells that have been in contact with MPs during 15 min only can be aggregated, and also why removing the EPS from cells does not decrease significantly the separation efficiency. To this end, we performed force-spectroscopy experiments to probe the interactions between single *C. vulgaris* cells and Model-MPs. In these experiments, cells have been washed to remove the EPS from the surface, this way it will be possible to directly probe the interactions between the cell's interface and the Model-MPs. For that, we used FluidFM technology, where single *C. vulgaris* cells are aspirated at the aperture of FluidFM probes by exerting a negative pressure inside the microfluidic cantilever. This negative pressure, compared to classic single-cell force spectroscopy methods using AFM, has the advantage of keeping the cells stable on the cantilever even when in contact with a strongly adhesive surface (Demir et al., 2020). The results of these experiments are presented in Figure 8. In the case of µ-PE (Figure 8a), the retract force curves obtained present a single retract peak happening close to the contact point, similar to what was observed with bubbles, with an average force of 14.6 ± 15.3 nN (n = 2713 force curves with 8

cells and particles coming from 2 different cultures, adhesion values can be found in Supplementary Table 4). As for the interactions with bubbles, this force signature is typical of non-specific interactions, and most likely reflect hydrophobic interactions, rather strong, between *C. vulgaris* cells and µ-PE. Similar force curves were obtained for µ-Upcon-PE with a similar average adhesion force of 15.4 ± 15.8 nN (n = 3470 force curves with 10 cells and particles coming from 2 different cultures, adhesion values can be found in Supplementary Table 5) shown in Figure 8b. The adhesion forces are not significantly different at p-value of 0.05 (unpaired student test). This is in line with the previous flocculation/flotation experiments, incorporating UCNPs to the µ-PE does not affect their interaction with *C. vulgaris* cells. Thus, these results first show that there is indeed an interaction between cells and Model-MPs, and that these interactions are nonspecific and hydrophobic. Recently, we evaluated the hydrophobicity of *C. vulgaris* by measuring the interaction between air bubble and single *C. vulgaris* cells (Demir et al., 2021), and found an average adhesion force of 4.2 nN (Demir et al., 2021), showing that the surface of cells is not completely hydrophilic and has hydrophobic properties. It thus means that Model-MPs can interact with cells directly through a hydrophobic interaction. This is also in line with the bi-photon imaging experiment where microparticles directly in contact with cells can be observed. To verify that no other type of non-specific interactions are involved, like electrostatic interactions, additional force spectroscopy experiments were performed between *C. vulgaris* and µ-Upcon-PE at higher salt concentrations (Figure 8c). When we increase the salt concentration by adding 500 mM of NaCl in PBS buffer (0.137 M of NaCl) at pH 7.4, the charges present on *C. vulgaris* cells and Model-MPs are shielded. Although the average adhesion force recorded is 11.0 ± 9.0 nN (n = 1785 force curves with 6 cells and particles coming from 2 different cultures, adhesion values can be found in Supplementary Table 6), given the wide distribution of the values obtained, it is in the same range as for cells without salt addition. But still the difference is significant (unpaired t-test, p-value of 0.05), meaning that electrostatic interactions are involved, but they are not dominant compared to the hydrophobic interaction. An interesting point to note concerns the wide distribution of the adhesion values obtained in each case. This heterogeneity can

be explained by the fact that in each case we aspirated a different cell. As we have no control over the cell sizes depending on their age, the contact area in each case is different, resulting in different adhesion values. Also, this heterogeneity in the results may be associated with the surface structure of the Model-MPs which is irregular, perhaps modifying the contact area and the adhesion force recorded. Indeed, when we look at the adhesion forces obtained throughout the surface of the microparticles scanned, we can see that as the cantilever moves on the surface, the Model-MPs adhesion force does not stay constant over consecutive measurements (decreases or increases, Supplementary Figure S5). Finally, to confirm that the forces recorded are due to only interactions of cells with microparticles, we probed the interactions between *C. vulgaris* cells and the surfaces of Model-MPs are immobilized on, *i.e.*, PDMS. The results presented in Supplementary Figure S6a and S6b show that neither *C. vulgaris* - PDMS nor FluidFM cantilever-Model-MPs interaction occurs, confirming that the interactions described here indeed take place between cells and Model-MPs.

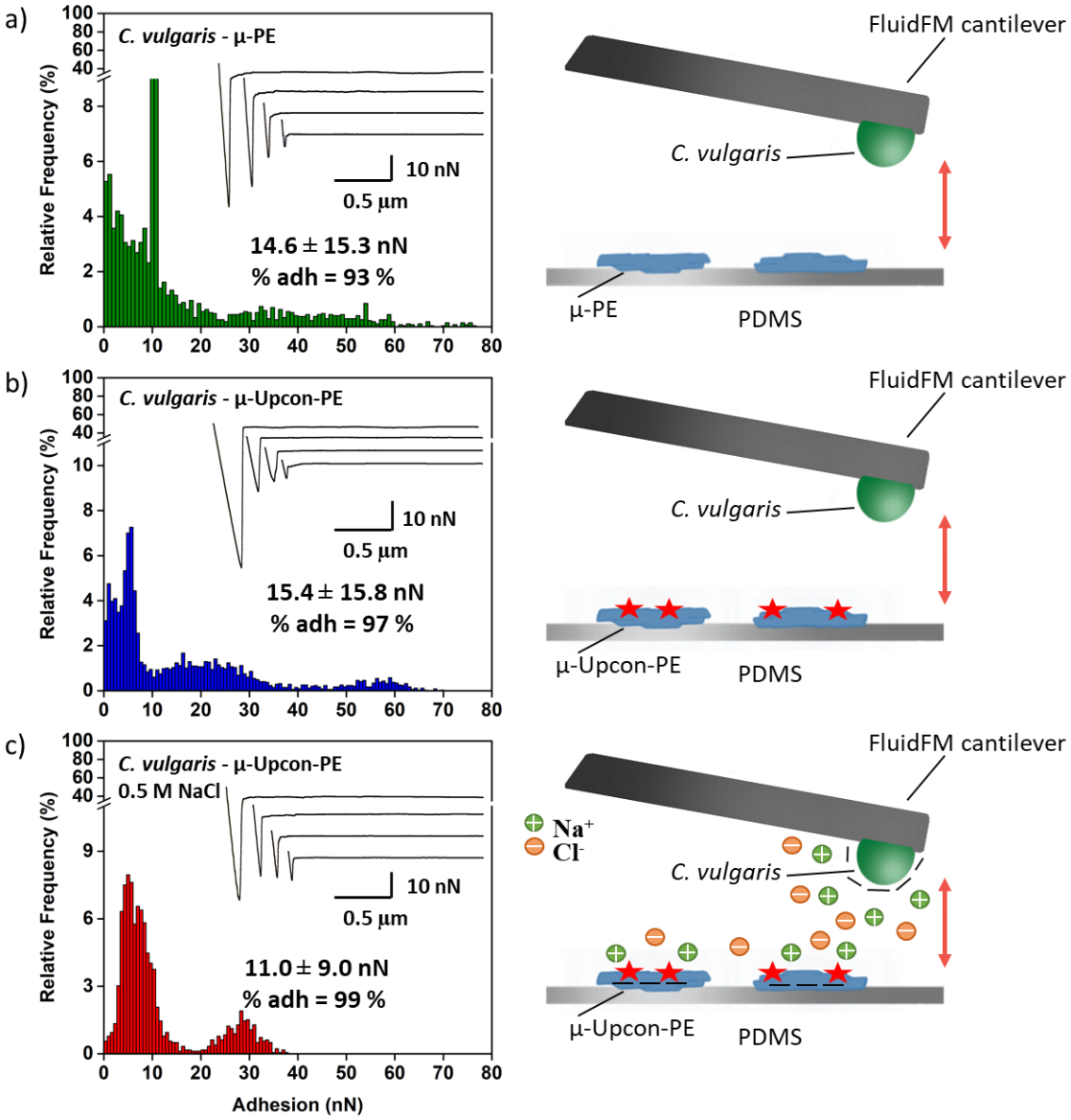

Figure 8: Probing the interactions between C. vulgaris cells and Model-MPs. *Histogram showing the distribution of adhesion forces Adhesion force histogram obtained for the interaction between C. vulgaris cells and a) μ-PE, b) μ-Upcon-PE, and c) μ-Upcon-PE after 0.5 M NaCl addition. Insets in a, b and c shows the representative force curves obtained during force spectroscopy experiments.*

Altogether, these results show that Model-MPs-induced aggregation can take place through different mechanisms. When cells have been grown in the presence of MPs, they use the MPs as a support for forming biofilms which triggers the production of EPS and the further aggregation of cells. However, MPs can also flocculate the cells by directly interacting with them, with their cell

surface directly and also with the small amount of EPS they produce at their surface in normal conditions.

4. Conclusions

The ubiquitous presence of plastic in all environmental compartments raises great concern about their potential negative impact on aquatic ecosystems in general. In recent decades, many research efforts have focused on understanding the inclusion, transport, and effects of microplastics on the aquatic trophic chain from zooplankton to mammals. However not much is known about the interaction of MPs with primary producers such as microalgae, which are the base of trophic chain. This study presents an original interdisciplinary work that allows for an understanding of the interactions between environmentally relevant models of MPs and microalgae cells and the consequences of such interaction. The biophysical characterization of the Model-MPs used in this study showed that these particles are rough and irregular, similar to the ones found in the environment, and also presents hydrophobic properties. Then, the combination of optical microscopy imaging assays and population-scale flocculation/flotation experiments allowed us to understand the role of MPs in the aggregation of cells. Our results showed that when cells are grown in the presence of MPs, they produce more EPS responsible for cell aggregation. However, the aggregation can also be induced by the direct contact between MPs and the cell surface or the EPS they produce naturally in normal culture conditions. This was confirmed by single-cell force spectroscopy experiments, which also led us to describe the physico-chemical nature of the interactions between Model-MPs and cells. Altogether, the experimental approach developed in this study has proven powerful to highlight the complexity of MPs-microalgae interactions and understand the role of MPs in the formation of cell aggregates. This new information are important to apprehend the impact of plastic pollution on aquatic ecosystems on a large scale.

Acknowledgements

C. F.-D. is a researcher at CNRS. C. F.-D. and C. C. acknowledge financial support for this work from the Agence Nationale de la Recherche, JCJC project FLOTALG (ANR-18-CE43-0001-01) and BLINK project (ANR-15-CE09-0020) respectively. The authors would like to thank Dr. Baptiste Amouroux for kindly supplying UCNPs.

Conflicts of interest

The authors declare no conflicts of interest.

References

Andrady, A., Neal, M., 2009. Applications and Societal Benefits of Plastics. Philosophical transactions of the Royal Society of London. Series B, Biological sciences 364, 1977–84. https://doi.org/10.1098/rstb.2008.0304

Andrady, A.L., Hamid, H., Torikai, A., 2011. Effects of solar UV and climate change on materials. Photochem Photobiol Sci 10, 292–300. https://doi.org/10.1039/c0pp90038a

ASTM E2865-12, 2018. Guide for Measurement of Electrophoretic Mobility and Zeta Potential of Nanosized Biological Materials. ASTM International, West Conshohocken, PA. https://doi.org/10.1520/E2865-12R18

Barbosa, A.B., 2009. Dynamics of living phytoplankton: implications for paleoenvironmental reconstructions, in: IOP Conference Series: Earth and Environmental Science. IOP Publishing, p. 012001. https://doi.org/10.1088/1755-1307/5/1/012001

Beardall, J., Raven, J.A., 2004. The potential effects of global climate change on microalgal photosynthesis, growth and ecology. Phycologia 43, 26–40. https://doi.org/10.2216/i0031-8884-43-1-26.1

713 Besson, A., Formosa-Dague, C., Guiraud, P., 2019. Flocculation-flotation harvesting mechanism of
714 Dunaliella salina: From nanoscale interpretation to industrial optimization. Water Research
715 155, 352–361. https://doi.org/10.1016/j.watres.2019.02.043
716 Bhagwat, G., Tran, T.K.A., Lamb, D., Senathirajah, K., Grainge, I., O'Connor, W., Juhasz, A., Palanisami,
717 T., 2021. Biofilms Enhance the Adsorption of Toxic Contaminants on Plastic Microfibers under
718 Environmentally Relevant Conditions. Environ. Sci. Technol. 55, 8877–8887.
719 https://doi.org/10.1021/acs.est.1c02012
720 Binnig, G., Quate, C.F., Gerber, Ch., 1986. Atomic Force Microscope. Phys. Rev. Lett. 56, 930–933.
721 https://doi.org/10.1103/PhysRevLett.56.930
722 Bravo M, Astudillo JC, Lancellotti D, Luna-Jorquera G, Valdivia N, Thiel M, 2011. Rafting on abiotic
723 substrata: properties of floating items and their influence on community succession. Mar
724 Ecol Prog Ser 439, 1–17. https://doi.org/10.3354/meps09344
725 Carson, H.S., Nerheim, M.S., Carroll, K.A., Eriksen, M., 2013. The plastic-associated microorganisms of
726 the North Pacific Gyre. Marine Pollution Bulletin 75, 126–132.
727 https://doi.org/10.1016/j.marpolbul.2013.07.054
728 Casabianca, S., Capellacci, S., Penna, A., Cangiotti, M., Fattori, A., Corsi, I., Ottaviani, M.F., Carloni, R.,
729 2020. Physical interactions between marine phytoplankton and PET plastics in seawater.
730 Chemosphere 238, 124560. https://doi.org/10.1016/j.chemosphere.2019.124560
731 Chopinet, L., Formosa, C., Rols, M.P., Duval, R.E., Dague, E., 2013. Imaging living cells surface and
732 quantifying its properties at high resolution using AFM in QI™ mode. Micron 48, 26–33.
733 https://doi.org/10.1016/j.micron.2013.02.003
734 Cid, Á., Prado, R., Rioboo, C., Suarez-Bregua, P., Herrero, C., 2012. Use of microalgae as biological
735 indicators of pollution: looking for new relevant cytotoxicity endpoints 311–323.
736 Cole, M., Lindeque, P., Fileman, E., Halsband, C., Goodhead, R., Moger, J., Galloway, T.S., 2013.
737 Microplastic Ingestion by Zooplankton. Environ. Sci. Technol. 47, 6646–6655.
738 https://doi.org/10.1021/es400663f

739 Cole, M., Lindeque, P., Halsband, C., Galloway, T.S., 2011. Microplastics as contaminants in the
740 marine environment: A review. Marine Pollution Bulletin 62, 2588–2597.
741 https://doi.org/10.1016/j.marpolbul.2011.09.025
742 Cunha, C., Faria, M., Nogueira, N., Ferreira, A., Cordeiro, N., 2019. Marine vs freshwater microalgae
743 exopolymers as biosolutions to microplastics pollution. Environmental Pollution 249, 372–
744 380. https://doi.org/10.1016/j.envpol.2019.03.046
745 Dague, E., Alsteens, D., Latgé, J.-P., Verbelen, C., Raze, D., Baulard, A.R., Dufrêne, Y.F., 2007. Chemical
746 Force Microscopy of Single Live Cells. Nano Lett. 7, 3026–3030.
747 https://doi.org/10.1021/nl071476k
748 Demir, I., Blockx, J., Dague, E., Guiraud, P., Thielemans, W., Muylaert, K., Formosa-Dague, C., 2020.
749 Nanoscale Evidence Unravels Microalgae Flocculation Mechanism Induced by Chitosan. ACS
750 Appl. Bio Mater. 3, 8446–8459. https://doi.org/10.1021/acsabm.0c00772
751 Demir, I., Lüchtefeld, I., Lemen, C., Dague, E., Guiraud, P., Zambelli, T., Formosa-Dague, C., 2021.
752 Probing the interactions between air bubbles and (bio)interfaces at the nanoscale using
753 FluidFM technology. Journal of Colloid and Interface Science 604, 785–797.
754 https://doi.org/10.1016/j.jcis.2021.07.036
755 Demir-Yilmaz, I., Guiraud, P., Formosa-Dague, C., 2021. The contribution of Atomic Force Microscopy
756 (AFM) in microalgae studies: A review. Algal Research 60, 102506.
757 https://doi.org/10.1016/j.algal.2021.102506
758 Dong, D., Zhang, L., Guo, Z., Hua, X., 2017. The role of extracellular polymeric substances on the
759 sorption of pentachlorophenol onto natural biofilms in different incubation times: a
760 fluorescence study. Chemistry and Ecology 33, 131–142.
761 https://doi.org/10.1080/02757540.2017.1281253
762 EPA US, 2016. White Paper: A Summary of the Literature on the Chemical Toxicity of Plastics
763 Pollution on Aquatic Life and Aquatic-Dependent Wildlife [WWW Document]. United State

764 Environmental Protection Agency. URL https://www.epa.gov/wqc/white-paper-summary-
765 literature-chemical-toxicity-plastics-pollution-aquatic-life-and-aquatic (accessed 10.17.21).
766 Formosa-Dague, C., Duval, R.E., Dague, E., 2018. Cell biology of microbes and pharmacology of
767 antimicrobial drugs explored by Atomic Force Microscopy. Seminars in Cell & Developmental
768 Biology, Application of Atomic Force Microscopy in cell biology 73, 165–176.
769 https://doi.org/10.1016/j.semcdb.2017.06.022
770 GESAMP, 2016. Sources, Fate and Effects of Microplastics in the Marine Environment (Part 2)
771 (Journal Series GESAMP Reports and Studies GESAMP Reports and Studies No. 93).
772 Geyer, R., Jambeck, J.R., Law, K.L., 2017. Production, use, and fate of all plastics ever made. Science
773 advances 3, e1700782. https://doi.org/10.1126/sciadv.1700782.
774 Gigault, J., El Hadri, H., Nguyen, B., Grassl, B., Rowenczyk, L., Tufenkji, N., Feng, S., Wiesner, M., 2021.
775 Nanoplastics are neither microplastics nor engineered nanoparticles. Nat. Nanotechnol. 16,
776 501–507. https://doi.org/10.1038/s41565-021-00886-4
777 Glibert, P.M., Icarus Allen, J., Artioli, Y., Beusen, A., Bouwman, L., Harle, J., Holmes, R., Holt, J., 2014.
778 Vulnerability of coastal ecosystems to changes in harmful algal bloom distribution in
779 response to climate change: projections based on model analysis. Global change biology 20,
780 3845–3858. https://doi.org/10.1111/gcb.12662
781 Gregory, M.R., Ryan, P.G., 1997. Pelagic plastics and other seaborne persistent synthetic debris: a
782 review of Southern Hemisphere perspectives. Marine debris 49–66.
783 https://doi.org/10.1007/978-1-4613-8486-1_6
784 Gu, B., Zhang, Q., 2018. Recent Advances on Functionalized Upconversion Nanoparticles for
785 Detection of Small Molecules and Ions in Biosystems. Advanced Science 5, 1700609.
786 https://doi.org/10.1002/advs.201700609
787 Guillard, R.R.L., Lorenzen, C.J., 1972. Yellow-green algae with chlorophyllide C2. Journal of Phycology
788 8, 10–14.

789 Harrison, J.P., Schratzberger, M., Sapp, M., Osborn, A.M., 2014. Rapid bacterial colonization of low-
790 density polyethylene microplastics in coastal sediment microcosms. BMC Microbiology 14,
791 232. https://doi.org/10.1186/s12866-014-0232-4
792 Hopes, A., Mock, T., 2015. Evolution of microalgae and their adaptations in different marine
793 ecosystems. eLS 1–9. https://doi.org/10.1002/9780470015902.a0023744
794 Horton, A.A., Walton, A., Spurgeon, D.J., Lahive, E., Svendsen, C., 2017. Microplastics in freshwater
795 and terrestrial environments: evaluating the current understanding to identify the
796 knowledge gaps and future research priorities. Science of the total environment 586, 127–
797 141. https://doi.org/10.1016/j.scitotenv.2017.01.190
798 Hutter, J.L., Bechhoefer, J., 1993. Calibration of atomic-force microscope tips. Review of Scientific
799 Instruments 64, 1868–1873. https://doi.org/10.1063/1.1143970
800 Irving, T.E., Allen, D.G., 2011. Species and material considerations in the formation and development
801 of microalgal biofilms. Appl Microbiol Biotechnol 92, 283–294.
802 https://doi.org/10.1007/s00253-011-3341-0
803 Jorissen, F., 2014. Colonization by the benthic foraminifer Rosalina (Tretomphalus) concinna of
804 Mediterranean drifting plastics, in: Marine Litter in the Mediterranean and Black Seas, CIESM
805 Workshop Monographs. pp. 87–95.
806 Kang, J., Zhou, L., Duan, X., Sun, H., Ao, Z., Wang, S., 2019. Degradation of Cosmetic Microplastics via
807 Functionalized Carbon Nanosprings. Matter 1, 745–758.
808 https://doi.org/10.1016/j.matt.2019.06.004
809 Kokalj, A.J., Hartmann, N.B., Drobne, D., Potthoff, A., Kühnel, D., 2021. Quality of nanoplastics and
810 microplastics ecotoxicity studies: Refining quality criteria for nanomaterial studies. Journal of
811 Hazardous Materials 415, 125751. https://doi.org/10.1016/j.jhazmat.2021.125751
812 Lagarde, F., Olivier, O., Zanella, M., Daniel, P., Hiard, S., Caruso, A., 2016. Microplastic interactions
813 with freshwater microalgae: Hetero-aggregation and changes in plastic density appear

814 strongly dependent on polymer type. Environmental Pollution 215, 331–339.
815 https://doi.org/10.1016/j.envpol.2016.05.006
816 Liu, G., Jiang, R., You, J., Muir, D.C.G., Zeng, E.Y., 2020. Microplastic Impacts on Microalgae Growth:
817 Effects of Size and Humic Acid. Environ. Sci. Technol. 54, 1782–1789.
818 https://doi.org/10.1021/acs.est.9b06187
819 Liu, X., Sun, P., Qu, G., Jing, J., Zhang, T., Shi, H., Zhao, Y., 2021. Insight into the characteristics and
820 sorption behaviors of aged polystyrene microplastics through three type of accelerated
821 oxidation processes. Journal of Hazardous Materials 407, 124836.
822 https://doi.org/10.1016/j.jhazmat.2020.124836
823 Lobelle, D., Cunliffe, M., 2011. Early microbial biofilm formation on marine plastic debris. Marine
824 Pollution Bulletin 62, 197–200. https://doi.org/10.1016/j.marpolbul.2010.10.013
825 Long, M., Moriceau, B., Gallinari, M., Lambert, C., Huvet, A., Raffray, J., Soudant, P., 2015.
826 Interactions between microplastics and phytoplankton aggregates: Impact on their
827 respective fates. Marine Chemistry 175, 39–46.
828 https://doi.org/10.1016/j.marchem.2015.04.003
829 Long, M., Paul-Pont, I., Hégaret, H., Moriceau, B., Lambert, C., Huvet, A., Soudant, P., 2017.
830 Interactions between polystyrene microplastics and marine phytoplankton lead to species-
831 specific hetero-aggregation. Environmental Pollution 228, 454–463.
832 https://doi.org/10.1016/j.envpol.2017.05.047
833 Mao, Y., Ai, H., Chen, Y., Zhang, Z., Zeng, P., Kang, L., Li, W., Gu, W., He, Q., Li, H., 2018.
834 Phytoplankton response to polystyrene microplastics: Perspective from an entire growth
835 period. Chemosphere 208, 59–68. https://doi.org/10.1016/j.chemosphere.2018.05.170
836 Masó, M., Garcés, E., Pagès, F., Camp, J., 2003. Drifting plastic debris as a potential vector for
837 dispersing Harmful Algal Bloom (HAB) species. Scientia Marina 67, 107–111.
838 https://doi.org/10.3989/scimar.2003.67n1107

839 Meister, A., Gabi, M., Behr, P., Studer, P., Vörös, J., Niedermann, P., Bitterli, J., Polesel-Maris, J., Liley,
840 M., Heinzelmann, H., Zambelli, T., 2009. FluidFM: Combining Atomic Force Microscopy and
841 Nanofluidics in a Universal Liquid Delivery System for Single Cell Applications and Beyond.
842 Nano Lett. 9, 2501–2507. https://doi.org/10.1021/nl901384x
843 Nava, V., Leoni, B., 2021. A critical review of interactions between microplastics, microalgae and
844 aquatic ecosystem function. Water Research 188, 116476.
845 https://doi.org/10.1016/j.watres.2020.116476
846 Oberbeckmann, S., Löder, M.G., Labrenz, M., 2015. Marine microplastic-associated biofilms–a
847 review. Environmental chemistry 12, 551–562. https://doi.org/10.1071/EN15069
848 Peng, L., Fu, D., Qi, H., Lan, C.Q., Yu, H., Ge, C., 2020. Micro- and nano-plastics in marine
849 environment: Source, distribution and threats — A review. Science of The Total Environment
850 698, 134254. https://doi.org/10.1016/j.scitotenv.2019.134254
851 Phuong, N.N., Zalouk-Vergnoux, A., Poirier, L., Kamari, A., Châtel, A., Mouneyrac, C., Lagarde, F.,
852 2016. Is there any consistency between the microplastics found in the field and those used in
853 laboratory experiments? Environmental Pollution 211, 111–123.
854 https://doi.org/10.1016/j.envpol.2015.12.035
855 Pillet, F., Chopinet, L., Formosa, C., Dague, É., 2014. Atomic Force Microscopy and pharmacology:
856 From microbiology to cancerology. Biochimica et Biophysica Acta (BBA) - General Subjects
857 1840, 1028–1050. https://doi.org/10.1016/j.bbagen.2013.11.019
858 Plastics Europe, 2020. Plastics - the Facts 2020.
859 Prata, J.C., Lavorante, B.R.B.O., B.S.M. Montenegro, M. da C., Guilhermino, L., 2018. Influence of
860 microplastics on the toxicity of the pharmaceuticals procainamide and doxycycline on the
861 marine microalgae Tetraselmis chuii. Aquatic Toxicology 197, 143–152.
862 https://doi.org/10.1016/j.aquatox.2018.02.015
863 Reddy, K.J., Soper, B.W., Tang, J., Bradley, R.L., 1996. Phenotypic variation in exopolysaccharide
864 production in the marine, aerobic nitrogen-fixing unicellular cyanobacterium Cyanothece sp.

865 World Journal of Microbiology & Biotechnology 12, 311–318.
866 https://doi.org/10.1007/BF00340206
867 Reisser, J., Shaw, J., Hallegraeff, G., Proietti, M., Barnes, D.K.A., Thums, M., Wilcox, C., Hardesty, B.D.,
868 Pattiaratchi, C., 2014. Millimeter-Sized Marine Plastics: A New Pelagic Habitat for
869 Microorganisms and Invertebrates. PLOS ONE 9, e100289.
870 https://doi.org/10.1371/journal.pone.0100289
871 Rowenczyk, L., Dazzi, A., Deniset-Besseau, A., Beltran, V., Goudounèche, D., Wong-Wah-Chung, P.,
872 Boyron, O., George, M., Fabre, P., Roux, C., Mingotaud, A.F., Halle, A. ter, 2020.
873 Microstructure Characterization of Oceanic Polyethylene Debris. Environ. Sci. Technol. 54,
874 4102–4109. https://doi.org/10.1021/acs.est.9b07061
875 Rowenczyk, L., Leflaive, J., Clergeaud, F., Minet, A., Ferriol, J., Gauthier, L., Gigault, J., Mouchet, F.,
876 Ory, D., Pinelli, E., Albignac, M., Roux, C., Mingotaud, A.F., Silvestre, J., Ten-Hage, L., Ter
877 Halle, A., 2021. Heteroaggregates of Polystyrene Nanospheres and Organic Matter:
878 Preparation, Characterization and Evaluation of Their Toxicity to Algae in Environmentally
879 Relevant Conditions. Nanomaterials (Basel) 11, 482. https://doi.org/10.3390/nano11020482
880 Rubin, A.E., Sarkar, A.K., Zucker, I., 2021. Questioning the suitability of available microplastics models
881 for risk assessment – A critical review. Science of The Total Environment 788, 147670.
882 https://doi.org/10.1016/j.scitotenv.2021.147670
883 Rummel, C.D., Jahnke, A., Gorokhova, E., Kühnel, D., Schmitt-Jansen, M., 2017. Impacts of Biofilm
884 Formation on the Fate and Potential Effects of Microplastic in the Aquatic Environment.
885 Environ. Sci. Technol. Lett. 4, 258–267. https://doi.org/10.1021/acs.estlett.7b00164
886 Shiraishi, H., 2015. Association of heterotrophic bacteria with aggregated Arthrospira platensis
887 exopolysaccharides: implications in the induction of axenic cultures. Bioscience,
888 Biotechnology, and Biochemistry 79, 331–341.
889 https://doi.org/10.1080/09168451.2014.972333

890 Singh, U.B., Ahluwalia, A.S., 2013. Microalgae: a promising tool for carbon sequestration. Mitigation
891 and Adaptation Strategies for Global Change 18, 73–95. https://doi.org/10.1007/s11027-012-
892 9393-3
893 Sjollema, S.B., Redondo-Hasselerharm, P., Leslie, H.A., Kraak, M.H.S., Vethaak, A.D., 2016. Do plastic
894 particles affect microalgal photosynthesis and growth? Aquat Toxicol 170, 259–261.
895 https://doi.org/10.1016/j.aquatox.2015.12.002
896 Song, C., Liu, Z., Wang, C., Li, S., Kitamura, Y., 2020. Different interaction performance between
897 microplastics and microalgae: The bio-elimination potential of Chlorella sp. L38 and
898 Phaeodactylum tricornutum MASCC-0025. Sci Total Environ 723, 138146.
899 https://doi.org/10.1016/j.scitotenv.2020.138146
900 Takahashi, T., 2019. Routine Management of Microalgae Using Autofluorescence from Chlorophyll.
901 Molecules. https://doi.org/10.3390/molecules24244441
902 Tang, Y.Z., Dobbs, F.C., 2007. Green Autofluorescence in Dinoflagellates, Diatoms, and Other
903 Microalgae and Its Implications for Vital Staining and Morphological Studies. Applied and
904 Environmental Microbiology. https://doi.org/10.1128/AEM.01741-06
905 ter Halle, A., Ladirat, L., Gendre, X., Goudouneche, D., Pusineri, C., Routaboul, C., Tenailleau, C.,
906 Duployer, B., Perez, E., 2016. Understanding the Fragmentation Pattern of Marine Plastic
907 Debris. Environ. Sci. Technol. 50, 5668–5675. https://doi.org/10.1021/acs.est.6b00594
908 Tunali, M., Uzoefuna, E.N., Tunali, M.M., Yenigun, O., 2020. Effect of microplastics and microplastic-
909 metal combinations on growth and chlorophyll a concentration of Chlorella vulgaris. Science
910 of The Total Environment 743, 140479. https://doi.org/10.1016/j.scitotenv.2020.140479
911 Vergnes, J.B., Gernigon, V., Guiraud, P., Formosa-Dague, C., 2019. Bicarbonate Concentration Induces
912 Production of Exopolysaccharides by Arthrospira platensis That Mediate Bioflocculation and
913 Enhance Flotation Harvesting Efficiency. ACS Sustainable Chem. Eng. 7, 13796–13804.
914 https://doi.org/10.1021/acssuschemeng.9b01591

915 Wingender, J., Neu, T.R., Flemming, H.-C. (Eds.), 1999a. Microbial Extracellular Polymeric Substances:
916 Characterization, Structure and Function. Springer-Verlag, Berlin Heidelberg.
917 https://doi.org/10.1007/978-3-642-60147-7
918 Wingender, J., Neu, T.R., Flemming, H.-C., 1999b. What are Bacterial Extracellular Polymeric
919 Substances?, in: Wingender, J., Neu, T.R., Flemming, H.-C. (Eds.), Microbial Extracellular
920 Polymeric Substances: Characterization, Structure and Function. Springer, Berlin, Heidelberg,
921 pp. 1–19. https://doi.org/10.1007/978-3-642-60147-7_1
922 Wu, Y., Guo, P., Zhang, X., Zhang, Y., Xie, S., Deng, J., 2019. Effect of microplastics exposure on the
923 photosynthesis system of freshwater algae. Journal of Hazardous Materials 374, 219–227.
924 https://doi.org/10.1016/j.jhazmat.2019.04.039
925 Xiao, J., Dufrêne, Y.F., 2016. Optical and force nanoscopy in microbiology. Nat Microbiol 1, 1–13.
926 https://doi.org/10.1038/nmicrobiol.2016.186
927 Xiao, R., Zheng, Y., 2016. Overview of microalgal extracellular polymeric substances (EPS) and their
928 applications. Biotechnology Advances 34, 1225–1244.
929 https://doi.org/10.1016/j.biotechadv.2016.08.004
930 Xiao, Y., Jiang, X., Liao, Y., Zhao, W., Zhao, P., Li, M., 2020. Adverse physiological and molecular level
931 effects of polystyrene microplastics on freshwater microalgae. Chemosphere 255, 126914.
932 https://doi.org/10.1016/j.chemosphere.2020.126914
933 Yakovenko, N., Amouroux, B., Albignac, M., Collin, F., Roux, C., Mingotaud, A.-F., Roblin, P., Coudret,
934 C., Halle, A.T., 2022. Top-Down Synthesis of Luminescent Microplastics and Nanoplastics by
935 Incorporation of Upconverting Nanoparticles for Environmental Assessment.
936 https://doi.org/10.26434/chemrxiv-2022-c5nlv
937 Yan, Z., Xu, L., Zhang, W., Yang, G., Zhao, Z., Wang, Y., Li, X., 2021. Comparative toxic effects of
938 microplastics and nanoplastics on Chlamydomonas reinhardtii: Growth inhibition, oxidative
939 stress, and cell morphology. Journal of Water Process Engineering 43, 102291.
940 https://doi.org/10.1016/j.jwpe.2021.102291

941 Zantis, L.J., Carroll, E.L., Nelms, S.E., Bosker, T., 2021. Marine mammals and microplastics: A
942 systematic review and call for standardisation. Environmental Pollution 269, 116142.
943 https://doi.org/10.1016/j.envpol.2020.116142
944 Zhang, C., Chen, X., Wang, J., Tan, L., 2017. Toxic effects of microplastic on marine microalgae
945 Skeletonema costatum: Interactions between microplastic and algae. Environmental
946 Pollution 220, 1282–1288. https://doi.org/10.1016/j.envpol.2016.11.005
947 Zhang, Y., Kang, S., Allen, S., Allen, D., Gao, T., Sillanpää, M., 2020. Atmospheric microplastics: A
948 review on current status and perspectives. Earth-Science Reviews 203, 103118.
949 https://doi.org/10.1016/j.earscirev.2020.103118
950
951